Soft Matter

PAPER

View Article Online
View Journal | View Issue

Cite this: *Soft Matter*, 2016, **12**, 3340

Finite cohesion due to chain entanglement in polymer melts

Shiwang Cheng,†[a] Yuyuan Lu,†[b] Gengxin Liu[a] and Shi-Qing Wang*[a]

Received 19th January 2016,
Accepted 19th February 2016

DOI: 10.1039/c6sm00142d

www.rsc.org/softmatter

Three different types of experiments, quiescent stress relaxation, delayed rate-switching during stress relaxation, and elastic recovery after step strain, are carried out in this work to elucidate the existence of a finite cohesion barrier against free chain retraction in entangled polymers. Our experiments show that there is little hastened stress relaxation from step-wise shear up to γ = 0.7 and step-wise extension up to the stretching ratio λ = 1.5 at any time before or after the Rouse time. In contrast, a noticeable stress drop stemming from the built-in barrier-free chain retraction is predicted using the GLaMM model. In other words, the experiment reveals a threshold magnitude of step-wise deformation below which the stress relaxation follows identical dynamics whereas the GLaMM or Doi–Edwards model indicates a monotonic acceleration of the stress relaxation dynamics as a function of the magnitude of the step-wise deformation. Furthermore, a sudden application of startup extension during different stages of stress relaxation after a step-wise extension, *i.e.* the delayed rate-switching experiment, shows that the geometric condensation of entanglement strands in the cross-sectional area survives beyond the reptation time τ_d that is over 100 times the Rouse time τ_R. Our results point to the existence of a cohesion barrier that can prevent free chain retraction upon moderate deformation in well-entangled polymer melts.

Introduction

Entangled polymers as a leading class of soft matter exhibit a rich variety of phenomena, some of which are common to other forms of soft matter while others are unique. When the basic building units are chain-like molecules, unique physics emerges to dictate rheological behavior. In particular, chain entanglement controls both linear and nonlinear rheological responses of high molecular-weight polymers.[1,2] Extensive studies on this subject have been made since de Gennes' reptation idea[3] over 40 years ago. Doi and Edwards treated intermolecular interactions in terms of a confining smooth tube in order to develop a microscopic model for polymer chain dynamics based on the reptation mechanism.[4–8] Today, the Doi–Edwards tube model is widely used as the standard model to not only depict the quiescent polymer dynamics[9,10] but also explore the nonlinear rheological behavior of entangled polymer melts and solutions.[11–19] By construction, the confining tube represents the intermolecular interactions in the sense that a test chain in the tube undergoes initial affine deformation before barrier-less chain retraction on the Rouse time scale (τ_R) and restores equilibrium contour length. Such barrier-free chain retraction has two consequences: (a) an appreciable stress decline owing to the chain retraction at a time around τ_R; (b) the affine elastic deformation is negligibly low when the Rouse–Weissenberg number $Wi_R = \dot{\gamma}\tau_R$ or $\dot{\varepsilon}\tau_R \ll 1$.

Recently, particle tracking velocimetry (PTV)[20] has become available to complement the conventional rheometric characterization of the nonlinear behavior of entangled polymer solutions and melts. For well-entangled polymers, large deformation produces remarkable strain localization such as shear banding[21] and non-quiescent relaxation.[22] Although the constitutive continuum model can also show the emergence of shear banding upon startup shear[23–26] such calculations do not produce a molecular picture for shear banding. On the other hand, questions have emerged from recent molecular dynamics simulations concerning[27–31] whether the tube model's smoothed-out treatment of intermolecular interactions[32,33] may have oversimplified the essential (physical network) picture of entangled polymers undergoing large deformation.

Many studies of stress relaxation at large step strain have been carried out to validate the tube model[34–56] under the assumption that quiescent relaxation prevails. Slip-link models have also been applied to describe strain softening from step shear under the assumption of quiescent relaxation.[57–61] Unaware of any wall slip[62] and localized elastic yielding[22] that give rise to excessive strain softening, many experiments applied magnitudes of step strain that are too high to ensure quiescent relaxation.[63] At the

[a] *Department of Polymer Science, University of Akron, Akron, Ohio 44325-3909, USA. E-mail: swang@uakron.edu*
[b] *State Key Laboratory of Polymer Physics and Chemistry, Changchun Institute of Applied Chemistry, Chinese Academy of Sciences, Changchun 130022, Peoples' Republic of China*
† Authors contribute equally to this work.

end of interfacial yielding[62] (*i.e.* wall slip) or elastic yielding[64] in the bulk, the sample heals, recovering its linear-response relaxation dynamics, coinciding with the tube model's prediction beyond τ_R when the reptation dynamics dominate. When the magnitude of the step strain is low enough or the entangled polymers are inherently incapable of undergoing strain localization,[65,66] stress relaxation can take place quiescently.

In the present paper, we perform both step-wise simple-shear and uniaxial-extension of moderate magnitude so that the stress relaxation is guaranteed to occur quiescently. By avoiding strain localization, we can compare experimental observations with the GLaMM model.[15] In Fig. 7a and b of a previous paper[33] we only briefly mentioned the discrepancy between the shear stress relaxation and the DE tube model. Here we provide the missing details. More importantly, new experiments of step-wise extension have been carried out to examine the universality of the comparison. Both shear and extension tests show that there is no accelerated stress decline after a sizable step-wise strain, in contrast to the prediction of the tube model. Recently Graham *et al.* also acknowledged this discrepancy.[67] In the second part of this paper, we carry out uniaxial extension experiments to discuss the effect of geometric condensation and show that the effect survives for a longer period than the reptation time, rather than for a transient moment shorter than the Rouse time τ_R.

Experimental section

A. Material

All the present experiments in both shear and extension modes are based on one monodisperse entangled styrene–butadiene random copolymer rubber (SBR153K). It has an averaged molecular weight M_w = 161 kg mol^{-1} and contains 25.6% styrene and 74.4% butadiene, out of which 70% is vinyl. The SBR153K has PDI = 1.05.

B. Apparatus and methods

The linear viscoelastic properties of this sample are determined from small amplitude oscillatory shear measurements (SAOS) using a second-generation Advanced Rheometric Expansion System (ARES-G2). Fig. 1 shows the SAOS curves at a reference temperature of 30 °C. A terminal relaxation time or reptation time, τ_d = 1340 s, is estimated from the crossover frequency in the G' and G'' curves, and the elastic plateau modulus G_{pl} = 0.49 MPa can be read from Fig. 1, corresponding to M_e = 4.8 kg mol^{-1}. The number of entanglements per chain is estimated to be $Z = M_w/M_e \sim 33$. The Rouse relaxation time τ_R can be estimated by the different methods.[68] In particular, $\tau_{R\eta} = \left(\frac{6M\eta}{\pi^2\rho RT}\right)\left(\frac{M_c}{M}\right)^{2.5} = 12.3$ s and $\tau_{R\omega} = \left(\frac{aM}{1.111\rho RT}\right)^2 = 13$, where η is the zero-shear viscosity, ρ is the mass density taken as 0.93 × 10^3 kg m^{-3}, $M_c = 2M_e$, and a is the prefactor at higher frequencies for $G'(\omega) = a\omega^{1/2}$. These values happen to be close to $\tau_R = \tau_d/3Z$ = 13.5 s. All the experiments were done at 30 °C except for the elastic recovery experiments that were done at 25 °C where τ_d = 2578 s.

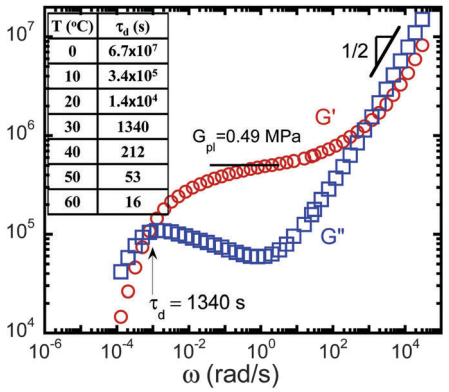

Fig. 1 Small amplitude oscillatory shear measurements of SBR153K at 30 °C. The reptation time is τ_d = 1340 s. The inset shows the Williams–Landel–Ferry (WLF) shift for this sample in the temperature range from 0 °C to 60 °C.

For the shear stress relaxation experiments, we modified the surfaces of 8 mm (in diameter) parallel steel plates to ensure the adhesion of the SBR melt on the shearing surfaces. Specifically, sand papers (Grit 240 Aluminum Oxide, Virginia Abrasives, Petersburg, VA) were adhered to the steel plates first. Then the sand-paper covered plates were heated to 70 °C along with the SBR melt with thickness of 1.0 mm. A pressure of around 100 g was applied between two plates for about five minutes. Subsequently, the sample was removed from the shear cell, and a thin layer of superglue (Loctite 498) was applied onto the sand paper before reloading with the surface-roughened sample. A period of at least 20 minutes was allowed to achieve good adhesion. Different strain rates from 0.1 s^{-1} to 10 s^{-1} were applied to examine the rate effect on the stress relaxation process. To mimic an ideal step strain experiment, we use the arbitrary wave (AW) mode to program the machine to reach to the setup strain within 0.04–0.06 s. For extensional experiments, a first generation of the Sentmanat Extensional Rheometer (SER) is mounted onto the ARES-G2 rotational rheometer. To avoid any slip, a thin layer of the superglue (Loctite 498) is used between the sample and the double drums on the SER. Different strain rates from 0.3 s^{-1} to 10 s^{-1} were applied to examine the rate effect.

Since the axial and torsion transducer compliance is K_A = 10^7 N m^{-1} and K_T = 1418 (mN) rad^{-1}, respectively, for ARES-G2, the axial response time (T_A) and torsion response time (T_T) can be estimated by: $T_A = 6\pi\eta R/(\alpha^3 K_A)$ and $T_T = 20\pi\eta R^3/(3\alpha K_T)$, where η is the zero shear viscosity of the testing sample, R is the radius of the plate and α is the angular displacement. In our tests, R = 4 mm, $\eta \sim G_{pl}\tau_d$. For γ = 1.0, $T_A/\tau_d \sim 0.2 < 1.0$ and $T_T/\tau_d \sim 0.001 \ll 1.0$. Thus, the transducer compliance should not affect our step strain measurements according to Venerus[52] and Vrentas and Graessley.[69]

In a delayed rate-switching experiment, at various stages during stress relaxation from a step-wise extension, the relaxing specimen is suddenly stretched again at a rate that produces a maximum in the engineering stress. In the elastic recovery experiments, an SER is mounted onto a controlled-torque rheometer (Physica MCR-301, Anton Paar). After reaching a

certain strain the sample is set stress free. The elastic recovery of the sample after deformation is captured, using a video camera connected to a digital video recorder, up to at least τ_d under the stress-free conditions on the SER.

Theoretical background

In order to explain the objectives and implications of our experiments, it is useful to review the prevailing theoretical description for stress relaxation of entangled polymer melts at moderate magnitude. By modeling the entanglement network in terms of a single chain in a tube, the tube model[8] has postulated that a test chain in the tube would actually retract on the Rouse time τ_R in a barrier-free manner upon a sudden startup deformation. Such chain retraction is to occur at any step strain, *i.e.* any value of γ or λ, to result in a dip in the relaxing stress. Sensitive rheometric instruments should be able to detect the tiny dip and allow the envisioned chain retraction to be identified by experiment.

According to the Doi–Edwards (DE) tube model, the stress relaxation takes place in two steps: (a) the contour length retracts back to its equilibrium value on τ_R, and (b) the chain orientation relaxes toward the isotropic distribution through the reptation on τ_d. The time-strain separability occurs when $\tau_R \ll \tau_d$. Specifically, for a large step-wise simple shear, the effective relaxation modulus is given by[8]

$$\sigma(\gamma,t)/\gamma = G(\gamma,t) = h(\gamma)\{1 + [\alpha(\gamma) - 1]\exp(-t/\tau_R)\}^2 G_{eq}(t), \quad (1)$$

where G_{eq} is the equilibrium relaxation modulus, and $[\alpha(\gamma) - 1]$ is the chain stretching contribution to the shear stress. The damping function $h(\gamma)$ is given in terms of the orientation function Q_{xy} as $h(\gamma) = Q_{xy}(\gamma)/\gamma \sim 1/(1 + \gamma^2/5)$. Similarly, for a large step-wise uniaxial extension, we have

$$\sigma(\lambda,t)/(\lambda^2 - 1/\lambda) = G^{ext}(\lambda,t) = g(\lambda)\{1 + [\alpha(\lambda) - 1]\exp(-t/\tau_R)\}^2 G_{eq}(t), \quad (2)$$

where $g(\lambda)$ is given by $f(\lambda)/(\lambda^2 - 1/\lambda)$, with $f(\lambda)$ given in eqn (7.140) and (7.141) of ref. 8. An analytical approximation of $\alpha(\gamma)$ and $\alpha(\lambda)$ is given in the inset of Fig. 2. As shown in Fig. 2, the stretching factor α varies with the shear strain γ and the stretching ratio λ respectively, where a $\sim$13% stress drop for a step-wise shear of $\gamma = 0.7$ and a $\sim$15% stress drop for a step-wise extension of $\lambda = 1.5$ can be found around τ_R. Such a stress decline should be readily observable in experiments if it occurs.

In this work, we compare our results with the original DE tube model and the latest version of the tube model, the GLaMM model. For the calculations of the original DE tube model (Fig. 6a and b), we measured $G_{eq}(t)$ from the linear-response experiments as shown in Fig. 3 and inset it into eqn (1) and (2). For the calculations of the GLaMM model (Fig. 6c and d), we choose the standard parameters[13,67] *i.e.*, $\alpha_d = 1.15$, $c_\nu = 0.1$ and $R_s = 2.0$ for the contour length fluctuations, constraint release and retraction terms, respectively, and impose the same strain histories as those of the experiments to ensure a direct comparison.

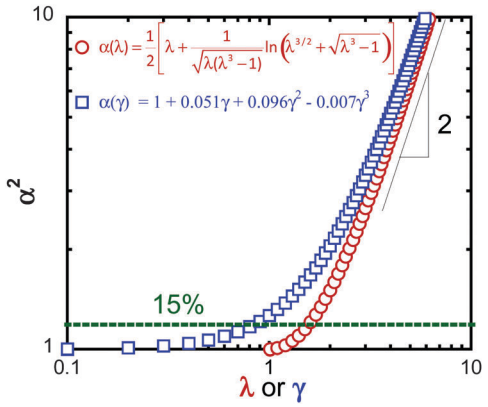

Fig. 2 The chain stretching factor α^2 *versus* the imposed strain for either shear or extension according to the tube model. The chain stretching would elevate the shear stress by 13% for $\gamma = 0.7$ and extensional stress by 15% for $\lambda = 1.5$.

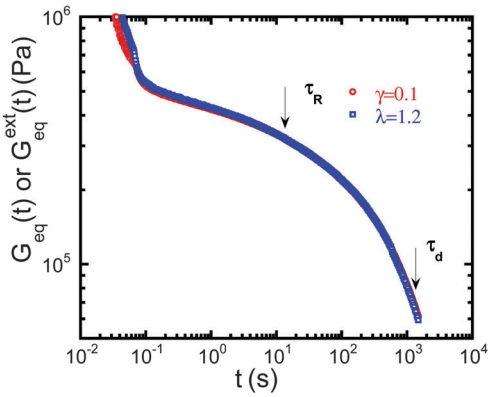

Fig. 3 Linear stress relaxation behavior comparisons of shear and extension. The relaxation moduli show identical time dependence throughout the relaxation. Here the prescribed strains of $\gamma = 0.1$ and $\lambda = 1.2$ were applied in the arbitrary wave mode and were reached within 0.03 s.

Results and discussion

A. Linear responses in shear and extension

We first carried out small step-wise strain in both shear and extension to determine the linear-response characteristics. Defining the equilibrium relaxation modulus as $G_{eq}(t) = \sigma(t)/\gamma(t)$ for simple shear and $G^{ext}_{eq}(t) = \sigma/(\lambda^2 - 1/\lambda)$ for uniaxial extension, we can present the stress relaxation as a function of time as shown in Fig. 3. The fact that the two curves overlap confirms that in this linear-response regime the preceding two formulas hold respectively for the small strains. In both experiments, it takes *ca.* 0.03 s to reach the prescribed strains of $\gamma = 0.1$ and $\lambda = 1.2$ respectively. The actual time dependence of $G_{eq}(t)$ and $G^{ext}_{eq}(t)$ is the same as expected.

B. Beyond linear response: large step-wise deformation

B.1 Experimental protocol. An ideal step strain involves the application of a prescribed strain within an infinitesimal amount of time. However, in experiments a step strain always

takes a finite amount of time. Fig. 4a–d examine the rate effect in both step-wise shear and extension and show that the long-time stress relaxation behavior is insensitive to the rate used (and the corresponding elapsed time) to produce the step-wise strain. If it takes t_1 to produce the step-wise strain, then as long as we are interested in the stress relaxation characteristics on time scales much longer than t_1, no information is lost. Since we are interested in the stress relaxation on time scales shorter than the Rouse time $\tau_R \sim 13$ s at 30 °C, for step shear we elect to use the arbitrary wave (AW) mode on the ARES-G2 that allows the preset strain to be applied within the shortest time, *i.e.*, around 0.02 to 0.04 s. For step extension, we apply a high Hencky rate $\dot{\varepsilon} = 10\ s^{-1}$.

B.2 Stress relaxation from large step strains. We examine the stress relaxation behavior at moderate magnitude of strain in both shear and extension respectively. Specifically, discrete step-wise shear tests were carried out involving the magnitude ranging from $\gamma = 0.1$ to 1.1, as shown in Fig. 5a. The inset of Fig. 5a shows that the prescribed strains were reached at around 0.04 s and there are inherent overshoots of the applied strain. The tiny vertical displacement of the stress curves relative to one another indicates that the shear stress $\sigma(t)$ does not increase exactly linearly with the applied strain γ. For the step-wise extension, the normalized $G^{ext}(t, \lambda)$ in Fig. 5b shows a significant vertical spread. This simply means that the tensile stress growth is weaker than the formula of $\sigma = G(\lambda^2 - 1/\lambda)$ from the rubber elasticity theory, which has been observed before in both entangled polymer melt[70] and crosslinked rubber.[71] The strain softening factors are summarized as $1.0 - G(t = 1\ s, \gamma)/G(t = 1\ s, \gamma = 0.1)$ for shear and $1.0 - G^{ext}(t = 1\ s, \lambda)/G(t = 1\ s, \lambda = 1.2)$ for uniaxial extension in Fig. 5c. Recently, similar strain softening was described in terms of tube dilation and chain retraction.[72] It will be interesting to compare the theoretical prediction with the strain softening observed in crosslinked rubbers, *i.e.*, the Mooney–Rivlin effect,[71] where chain retraction cannot take place. Any further discussion of the origin of this softening is beyond the scope of the present study.

To see more clearly how the stress relaxation varies with the magnitude of the step strain, *i.e.*, to compare the "shapes" of the relaxation modulus, we vertically shift the curves by normalizing the strain softening effect in Fig. 5a and b according to Fig. 5c to match at the initial times so that an effective relaxation modulus $G_{eff}(t)$ can be compared for different magnitudes as shown in Fig. 5d and e. Over the explored range, the $G_{eff}(t)$ shows little magnitude dependence, for shear strain from 0.1 to 0.7 (Fig. 5d) and for the stretching ratio from 1.2 to 1.7 (Fig. 5e). The lack of any strain dependence on the relaxation modulus G_{eff} up to $\gamma = 0.6$

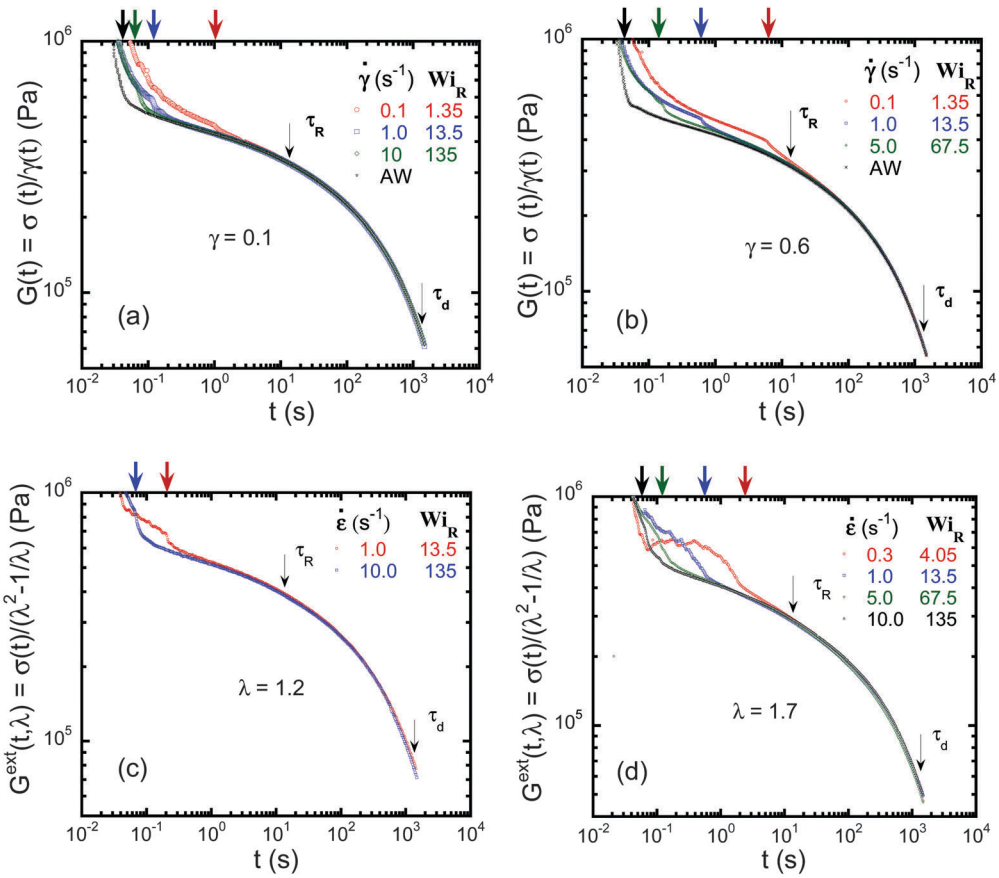

Fig. 4 Relaxation modulus obtained under different modes to impose the prescribed step strain for both simple shear (a) and (b) and uniaxial extension (c) and (d). Here AW designates the arbitrary wave mode where preset strain is produced in a rate as fast as the machine can achieve. For a strain of 0.1 and 0.6, it takes less than 0.04 s to reach. The other rates are clearly labeled inside each figure. The Rouse Weissenberg number is defined as $Wi_R = \dot{\gamma}\tau_R$ for shear and $Wi_R = \dot{\varepsilon}\tau_R$ for extension. The arrows indicate the time when the applied deformation terminates for each deformation rate.

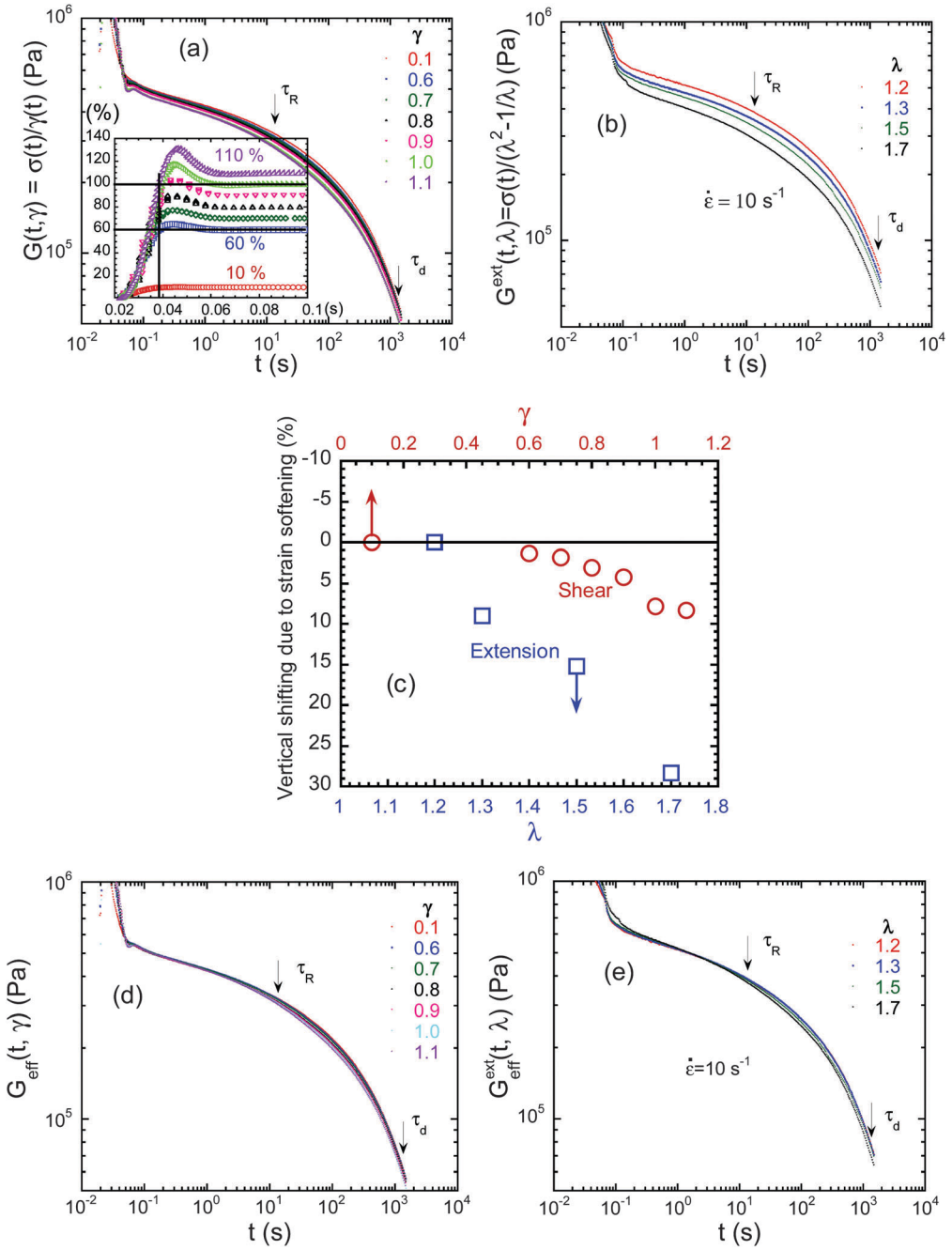

Fig. 5 (a) Relaxation modulus as a function of time for different magnitudes of the step-wise shear, ranging from γ = 0.1 to 1.1, imposed within 0.04–0.06 s. (b) Relaxation modulus as a function of time for different stretching ratios λ ranging from 1.2 to 1.7, imposed with a Hencky rate of 10 s^{-1}. (c) The amount of vertical shift due to strain softening. (d) and (e) replots of (a) and (b) after the vertical shifts according to (c).

as shown in Fig. 5d has justified the employment of the parallel-disc for the stress relaxation measurements that involve the imposition of varying strains radially across the sample. In other words, the parallel-plate measurements are rigorously valid for comparison with the theoretical prediction for $\gamma < 0.7$.

C. Comparison with the theoretical prediction: a cohesive barrier against barrier-free retraction

According to the DE tube model, the relaxation modulus $G(t)$ in eqn (1) and (2) drops below the equilibrium relaxation modulus G_{eq} around the Rouse time scale because barrier-free chain retraction occurs. The magnitude of the decrease, as a function of the magnitude of the step strain, is determined by the α factor of Fig. 2. Specifically, based on G_{eq} available from the experimental data in Fig. 3, we can plot the theoretical estimate (DE) for different magnitudes as shown in Fig. 6a and b. We also present the calculations of the GLaMM model in Fig. 6c and d.

To quantify the difference between Fig. 5d, e and 6a–d at relatively long times, we plot the ratios $G_{eff}(t, \gamma)/G_{eff}(t, \gamma = 0.1)$ and $G^{ext}_{eff}(t, \lambda)/G^{ext}_{eff}(t, \lambda = 1.2)$ as a function of γ and λ, respectively,

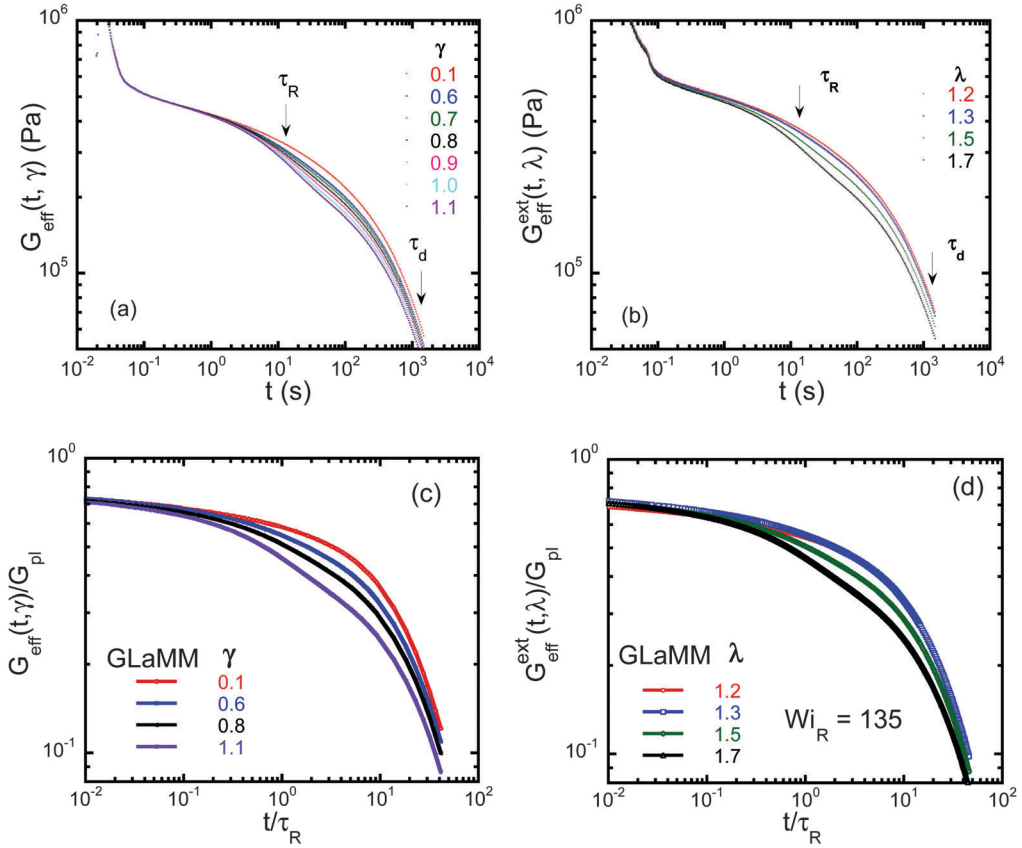

Fig. 6 DE tube model calculation of shear modulus for a range of γ from 0.1 to 1.1 (a), and extensional relaxation modulus for the stretching ratio λ ranging from 1.2 to 1.7 (b). The GLaMM model calculation of the shear relaxation modulus for a range of γ values from 0.1 to 1.1 (c), and the extensional relaxation modulus for the stretching ratio λ values ranging from 1.2 to 1.7 (d).

for $t = 5\tau_R$, $10\tau_R$, $20\tau_R$, $50\tau_R$, as shown in Fig. 7a and b. On one hand, the normalized relaxation modulus remains constant up to $\gamma = 0.6$ for step shear and up to $\lambda = 1.5$ for step extension, as indicated by the horizontal dashed lines in Fig. 7a and b. On the other hand, the tube model predicts a notable systematic downward deviation from the horizontal lines as shown by the red half-filled squares (the DE tube model) and green half-filled squares (the GLaMM model) respectively. The noticeable difference in Fig. 7a between the DE tube model and the GLaMM model may be expected. The chain stretching was incorporated into the DE model as an independent contribution to stress whereas the GLaMM treat chain stretching and orientation as coupled. Since the tube model anticipates a stress drop from barrier-free chain retraction at a time scale around τ_R,

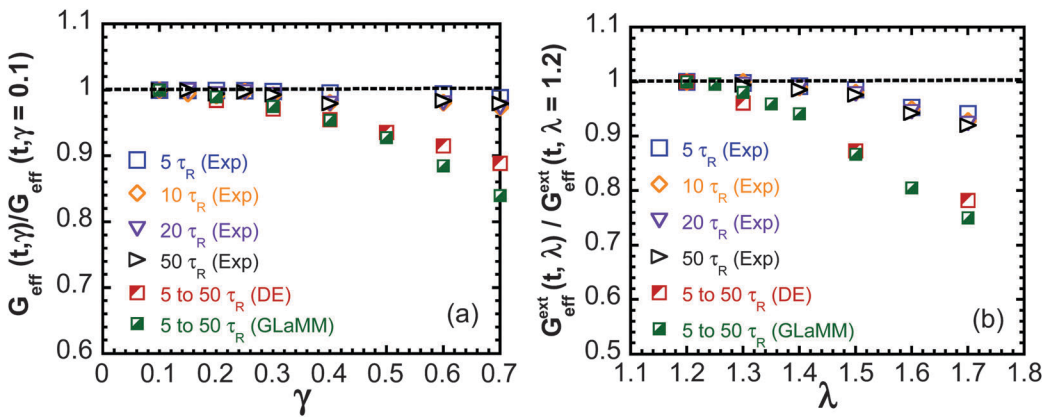

Fig. 7 Normalized relaxation moduli based on experiment, the original Doi–Edwards tube model and the GLaMM model at "long time" from $5\tau_R$ to $50\tau_R$ for both (a) shear and (b) extension. The results from both the DE tube model calculation and the GLaMM model calculation are identical at different times from 5 to $50\tau_R$.

we regard such differences to be qualitative, revealing the inadequacy of the basic premise of barrier-free chain retraction, upon which any version of the tube model was built. In other words, the experiment uncovers a new concept that we term "finite cohesion": the entanglement network would remain intact after fast external deformation unless the magnitude of the stepwise deformation exceeds a sizable magnitude. Our present work focuses on the identification of such a threshold since the elastic yielding behavior at higher magnitude (leading to strain localization) has been investigated previously for both stepwise shear[22] and extension.[73] As shown in Fig. 7a, the stress relaxation is independent of the strain up to $\gamma = 0.6$ in contradiction to the depictions by the GLaMM and DE models presented in Fig. 6a and c as well as in Fig. 7a. At higher strains, *i.e.*, for $\gamma > 0.7$, the cone-plate based measurements would be necessary. Alternatively, for the parallel-disk measurements, the GLaMM calculations of the stress relaxation can be carried out for the parallel-disk configuration. Given the sufficiently large discrepancy between the experiment and theory in Fig. 7a up to $\gamma = 0.6$, we deem it beyond the scope of this study to make such GLaMM calculations. Moreover, it is remarkable that the idea of finite cohesion associated with the entanglement network bears out for both shear and extension, illustrating the universality of the observed behavior.

To better understand the qualitative differences observed between experiments and the predictions of the tube model, we seek a more detailed analysis of the nature of the stress. According to the GLaMM model, both chain orientation and stretching contribute to the stress, which separate after the barrier-free chain retraction at τ_R. The orientational portion of the stress can be calculated by following a previous procedure[30] within the frame of the GLaMM model. As shown in Fig. 8a and b, the contributions of chain stretching to the shear stress quickly vanish around τ_R in all cases, with σ_{or}/σ converging to unity after $t/\tau_R = 1$. The convergence involves as much as 25% drop in the relaxing stress for $\gamma = 1.1$, and nearly 10% for $\gamma = 0.6$. It is this diminishing stretching component of the stress that causes the overall stress in the GLaMM model to show discernible dependence on the magnitude of the stepwise deformation.

However, the lack of accelerated stress relaxation in the experimental data up to a strain of around $\gamma = 0.6$ and an elongation ratio of around $\lambda = 1.5$ implies that chain retraction did not really take place after stepwise deformation at the low magnitude. Then, the essential question is why chain retraction could not occur at moderate strain magnitude. Since the chain retraction cannot take place on time scales much shorter than the reptation without either dragging the surrounding chains with it or altering its conformation, our experiments suggest that entanglement strands in the deformed network remain stretched at moderate magnitude of stepwise deformation, *i.e.*, chain retraction does not occur in a barrier-less fashion, which is consistent with the recent molecular dynamics simulations.[29–31] Therefore, we propose that there is a barrier due to interchain uncrossability to resist spontaneous chain retraction, of which the nature requires further investigation in the future. At higher magnitude, *e.g.*, beyond $\gamma = 0.6$ and $\lambda = 1.5$, when the stress relaxation quickens, the deformed strands still need to fight against the barrier. As a consequence, the stress relaxation is only moderately faster with increasing magnitude as shown in Fig. 7a and b, unlike the predictions of GLaMM that assumes barrier-less chain retraction.

D. Probing the state of chain entanglement during stress relaxation

To learn more about the stress relaxation process, we follow the same protocol previously applied to study the relaxation behavior after a step-wise shear of entangled solutions.[66] Namely, we carried out delayed rate-switching experiments to probe the change of the state of chain entanglement during stress relaxation from a step-wise extension. Specifically, after a step-wise extension to various magnitudes given by the stretching ratio $\lambda_1 = 1.2$, 1.5, 1.8 and 2.2 respectively, involving a Hencky rate $\dot{\varepsilon} = 1.0\ s^{-1}$, the specimen is allowed to relax for a period t_w starting from the end of the tensile deformation before another startup extension with $\dot{\varepsilon} = 0.3\ s^{-1}$ is imposed on the relaxing sample. Here the different waiting time t_w ranges from $\tau_R/2$ to several τ_d values.

To provide the necessary background, we first present in Fig. 9a the stress–strain curves at both $\dot{\varepsilon} = 0.3$ and $1.0\ s^{-1}$,

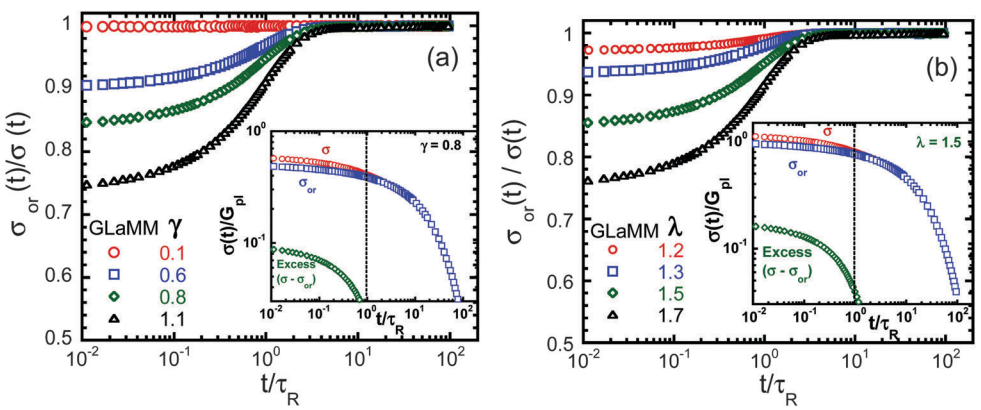

Fig. 8 Orientational contribution σ_{or} to the total stress σ for both (a) shear and (b) extension calculated by the GLaMM model. Note that insets are the total stress σ, the orientational stress σ_{or}, and excess stress $(\sigma - \sigma_{or})$ at $\gamma = 0.8$ for shear and $\lambda = 1.5$ for extension, respectively.

obtained from freshly loaded equilibrium samples. At $\dot{\varepsilon} = 1.0\ s^{-1}$, the engineering stress σ_{engr} only monotonically increases until rupture around $\lambda = 14$. At $\dot{\varepsilon} = 0.3\ s^{-1}$, there is a characteristic stress peak $\sigma_{engr0(max)}$ at 1.0 MPa. Here, we choose $\sigma_{engr} = F/A_0$ instead of true stress because the engineering stress maximum $\sigma_{engr(max)}$ is an effective macroscopic measure of the molecular events such as chain disentanglement.[74,75] During startup extension, the loss of entanglement strands competes with the growing stretch of the surviving strands. Thus, the peak of σ_{engr} signifies the global yielding of the entanglement network[74] when further stretching of the surviving entanglement strands is offset by the massive chain disentanglement. These features can be exploited to learn about the state of chain entanglement during stress relaxation.

Since up to $\lambda = 2.0$ the stress–strain curve does not deviate much from the linearity at an elongation rate of $\dot{\varepsilon} = 1.0\ s^{-1}$, the extension should be nearly affine. In affine deformation, there is a geometric condensation effect as indicated by the inset in Fig. 9a. The same (load-bearing) entanglement strands condense into a smaller cross-sectional area because of the homogeneous uniaxial extension. During relaxation, the condensation of the entanglement strands will disappear over time by molecular diffusion. Our delayed rate-switching experiment can actually quantify such a change in the state of entanglement by determining when the step-extended sample returns to the "non-condensed" equilibrium state, having a smaller cross-sectional area than the initial by a factor of λ. According to our understanding, the condensation effect may survive after step extension until the reptation time τ_d, as depicted in Fig. 9b. In contrast, if chain retraction takes place on the time scale of τ_R, the condensation should vanish for $t_w > \tau_R$ as shown in Fig. 9b by the cartoon below the stress relaxation curve.

If affine deformation prevails in the preceding step-wise extension to a stretching ratio of λ_1 and the same total number of the original entanglement strands would participate in resisting the subsequent startup extension even after a certain amount of waiting time t_w at λ_1, then we may see the same level of the tensile force although the cross-sectional area is now lower by a factor of λ_1. In other words, before the effect of geometric condensation vanishes through molecular diffusion, there is still the same number of load-bearing entanglement strands across the specimen in spite of the areal reduction by λ_1.

Therefore we probe the stress relaxation process after a step-wise extension by application of a startup extension with $\dot{\varepsilon} = 0.3\ s^{-1}$ at different stages of relaxation. Fig. 10a–d present these discrete delayed rate-switching experiments, where the engineering stress σ_{engr} at various stages is defined as the total tensile force F divided by the initial total cross-section area A_0: $\sigma_{engr} = F/A_0$. The fact that up to $t_w = 100$ s the startup extension produces a similar stress peak level for $\lambda_1 = 1.2$, 1.5 and 1.8 is an indication that (a) there is nearly affine deformation and (b) the corresponding effect of the geometric condensation persists up to $t_w = 100$ s.

We have used the value $\sigma_{engr(max)}$ to assess whether the original entanglement strands are still present and participate to resist the applied startup extension after various amounts of relaxation. The stress response eventually drops, consistent with the reduced cross-sectional area by λ_1, after full relaxation when the new entanglement strands are at the equilibrium density.

Treating the step-extended specimen as a "fresh" sample with an initial cross-sectional area of $A_0' = A_0/\lambda_1$, we plot the engineering stress $\sigma_{engr2} = F/A_0'$ arising from the startup extension as a function of time in Fig. 11a and b, where σ_{engr} from the startup extension on an equilibrium sample is also plotted as reference (solid dots). The fact that the curves represented by the open symbols systematically stay above the solid dots is consistent with the picture depicted in Fig. 9b. For $t_w \sim 1500\ s > \tau_d$ at $\lambda_1 = 1.2$, and $t_w = 7500\ s = 5.6\tau_d$ at $\lambda_1 = 1.8$, even though the peak value of σ_{engr2}, *i.e.*, $\sigma_{engr2(max)}$, has returned to $\sigma_{engr0(max)}$, the shape of these curves still deviates slightly from the original curve (solid

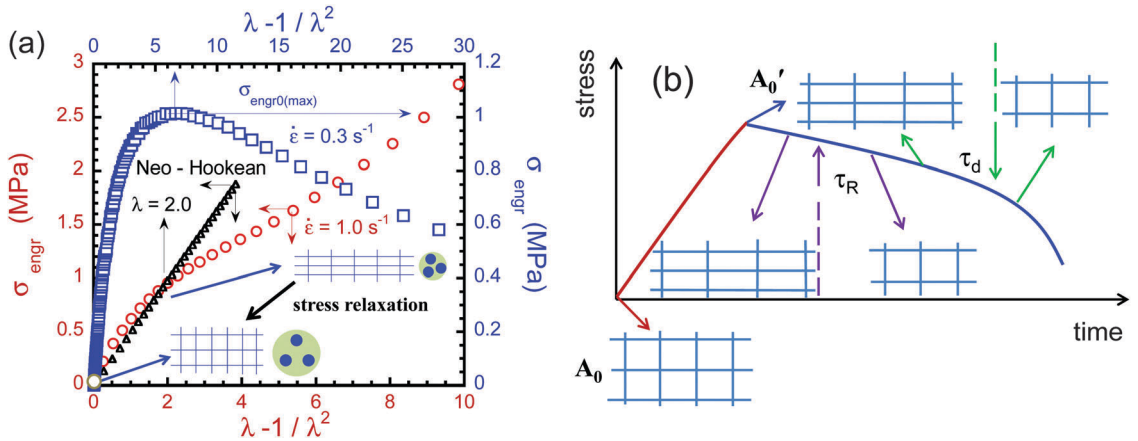

Fig. 9 (a) Engineering stress σ_{engr} *versus* the measure of extension, $\lambda - 1/\lambda^2$, for the two applied Hencky rates of 0.3 and 1.0 s^{-1}, respectively, plotted on double-*X* and double-*Y* axes. Up to $\lambda = 2.0$, the stress growth is essentially linear at $\dot{\varepsilon} = 1.0\ s^{-1}$. Thus, up to the elongation ratio of $\lambda = 2.0$, the affine deformation condition holds well. The inset illustrates the geometric condensation effect on the entanglement strands, where the dots represent the entanglement strands viewed in the transverse cross-section where the entanglement strand density is higher. (b) The states of the entanglement network at different stages before, during and after a step uniaxial extension. If chain retraction would take place at τ_R, the geometric condensation effect would be absent during much of the stress relaxation. Conversely, the geometric condensation effect will survive for moderate magnitude of the step extension if finite cohesion is present to prevent chain retraction. A_0 denotes the initial cross-section area and A_0' represents the cross-section area after step strain.

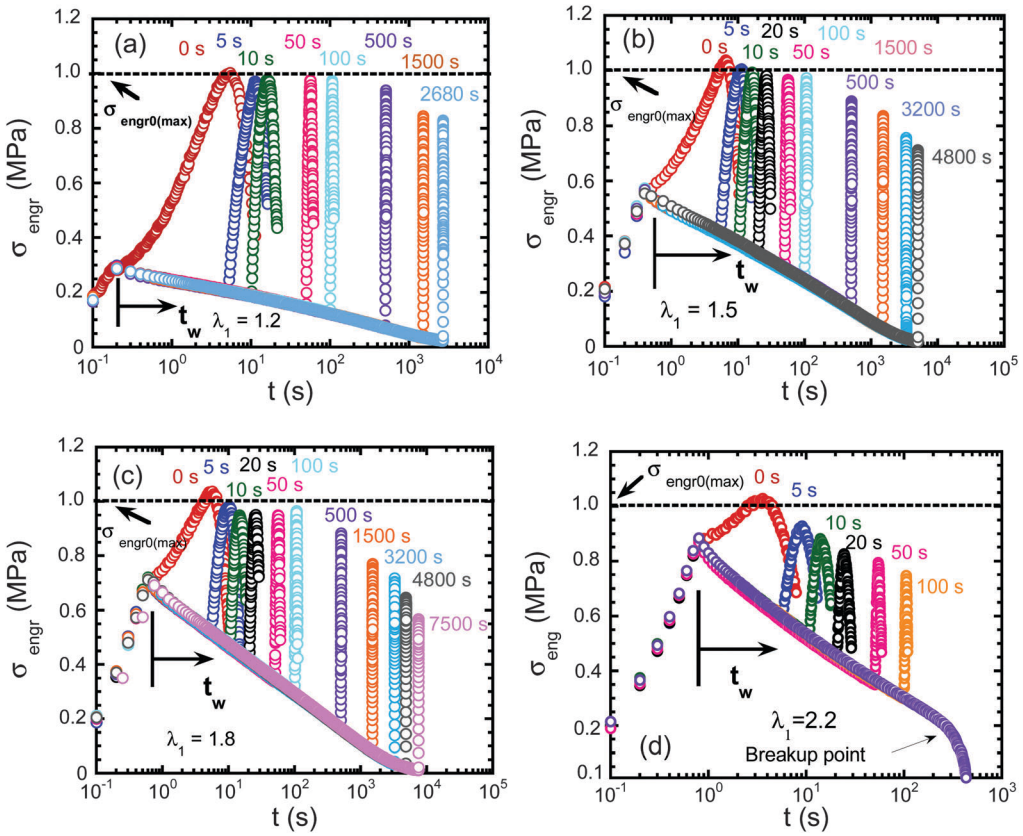

Fig. 10 (a–d) Delayed rate-switching (to $\dot{\varepsilon}$ = 0.3 s^{-1}) experiments during stress relaxation from step extension (produced with $\dot{\varepsilon}$ = 1.0 s^{-1}) of magnitude corresponding to λ_1 = 1.2, 1.5, 1.8 and 2.2 respectively, where the subsequent startup extension after a period of relaxation t_w produces a maximum in σ_{engr} as shown, along with the preceding stress build-up and relaxation data. In each of (a) to (c), $\sigma_{engr(max)}$ remains the constant close to $\sigma_{engr0(max)}$ in the first 100 s. Except for λ_1 = 1.2, $\sigma_{engr(max)}$ does not decrease to $\sigma_{engr0(max)}/\lambda_1$ within the reptation time τ_d. For λ_1 = 2.2, the specimen underwent breakup at t_w = 300 s due to localized elastic yielding. The elastic yielding[64] also causes $\sigma_{engr(max)}$ to decrease momentarily.

dots), indicating that the relaxing sample has not fully returned to the equilibrium state. This is consistent with the accumulating literature that reported longer recovery time than τ_d to the equilibrium state.[76]

Plotting the "normalized" peak stress $\sigma_{engr2(max)}$ read from such data as those in Fig. 11a and b as a function of t_w, we can more clearly demonstrate, in Fig. 12a, the effect of molecular relaxation on the geometric condensation. There are several remarkable features in Fig. 12a. First, $\sigma_{engr2(max)}$ remains essentially constant up to 100 s for λ_1 = 1.2, 1.5 and 1.8. In other words, $\sigma_{engr2(max)}$ remains higher than $\sigma_{engr0(max)}$ by a factor close to λ_1 for a period as long as eight times the Rouse time τ_R. Second, for λ_1 = 1.2, it takes about one reptation time τ (*i.e.*, $t_w \sim \tau_d$ = 1340 s) for $\sigma_{engr2(max)}$ to return to $\sigma_{engr0(max)}$, when the effect of the step extension completely disappears. Third, for λ_1 = 1.5 and 1.8, the peak stress remains higher than $\sigma_{engr0(max)}$ for t_w as long as (4–6)τ_d, which is hundred times longer than the Rouse time.

It is equally revealing to "renormalize" the peak stress level, *i.e.*, to simply plot $\sigma_{engr(max)} = \sigma_{engr2(max)}/\lambda_1$ *versus* the waiting time t_w as shown in Fig. 12b. First, we see that all the data up to λ_1 = 1.8 remain around $\sigma_{engr0(max)}$ = 1.0 MPa for $t_w < 100$ s although the relaxing tensile stress has decreased by a factor of two as shown in Fig. 10a to c. Had chain retraction occurred around the Rouse time τ_R = 13 s, the geometric condensation effect should have disappeared long before 100 s and $\sigma_{engr(max)}$ would have dropped below $\sigma_{engr0(max)}$ since the cross-sectional area is smaller by λ_1. Second, Fig. 12b is consistent with the idea of finite cohesion of the entanglement network. The initial overlapping of data for λ_1 = 1.2, 1.5 and 1.8 indicates that the entanglement network starts to return to its "non-condensed" state only after 100 s, independent of the value of λ_1. Third, except for λ_1 = 1.2, it takes several reptation times τ_d for the effect of step extension to vanish. In other words, the effect of the preceding extension remains strong even after a relaxation time of $t_w \sim \tau_d$. When the equilibrium state is recovered, the startup extension should produce a peak stress that is lower than $\sigma_{engr(max)}$ = 1.0 MPa by a factor of λ_1, *i.e.*, equal to $\sigma_{engr0(max)}/\lambda_1 = (1/\lambda_1)$ MPa because the specimen's cross-sectional area A_0' is smaller than the original A_0 by a factor of λ_1. The filled symbols on the right *Y* axis indicate these values. Lastly, there is a progressive decrease of the $\sigma_{engr2(max)}$ when λ_1 is as high as 2.2 as shown in Fig. 10d and 12a, suggesting a loss of load bearing strands or entanglements from the very beginning of the stress relaxation process. Such an observation is consistent with our observations in Fig. 7b and supports the idea that the cohesion barrier is finite and can be overcome when the elastic stress of a chain is high enough.[64]

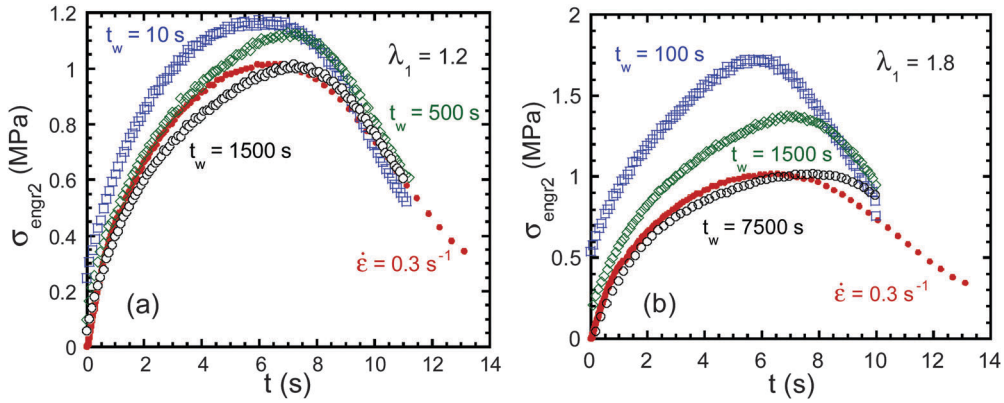

Fig. 11 Engineering stress σ_{engr2} as a function of time, resulting from the startup extension applied at various stages (designated by t_w) during stress relaxation from three different step extensions of (a) $\lambda_1 = 1.2$ and (b) $\lambda_1 = 1.8$ respectively. The solid dots represent the stress *vs.* time curve from an equilibrium sample (*i.e.*, $\lambda_1 = 0$) in terms of $\sigma_{engr} = F/A_0$.

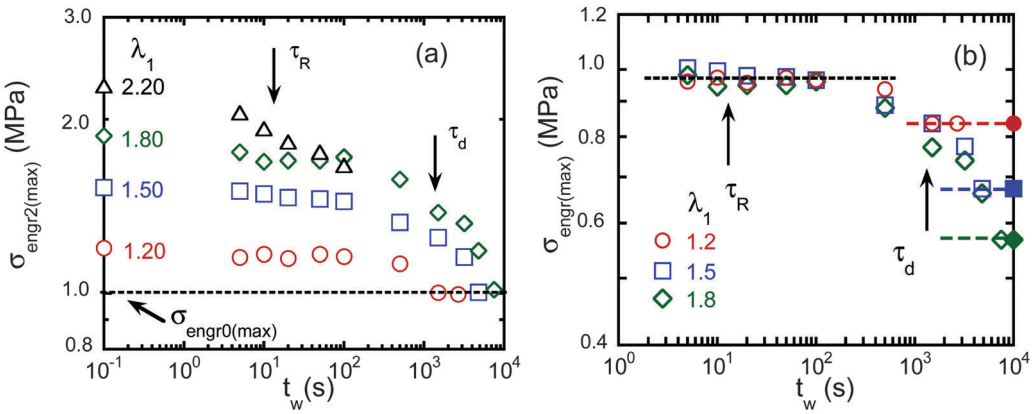

Fig. 12 (a) Engineering stress maximum from the startup extension applied during stress relaxation from the step extension of four different magnitudes, defined as the total tensile force F divided by the actual cross-sectional area A_0/λ_1. (b) Renormalized engineering stress maximum $\sigma_{engr(max)} = F_{max}/A_0 = \sigma_{engr2(max)}/\lambda_1$ as a function of the duration of the stress relaxation t_w. Here the filled symbols on the right-hand-side Y axis indicate the equilibrium values $\sigma_{engr0(max)}/\lambda_1$ that $\sigma_{engr(max)}$ is expected to reduce in the long time limit when the step-extended sample fully relaxes to the equilibrium state. For $\lambda_1 = 1.5$ and 1.8, it takes several τ_d values to reach $\sigma_{engr0(max)}/\lambda_1$. The dashed lines indicate the equilibirum state for each elongation ratio.

E. Quantifying the elastic state during startup extension: elastic recovery

When the Rouse–Weissenberg number $Wi_R = \dot{\varepsilon}\tau_R$ is below unity, the intermolecular griping force is negligible as suggested in a previous study of large extension behavior of entangled melt.[77] When $Wi_R < 1$, startup extension ceases to be affine beyond a stretching ratio $\lambda = \exp(Wi_R)$. According to the tube model, σ_{engr} exhibits a maximum because of the combination of saturated chain orientation and shrinkage of the cross-sectional area. In other words, the non-monotonicity does not signify any breakdown of the entanglement network. We carry out the elastic recovery experiment to further explore the concept of the cohesion associated with the chain entanglement as well as the concept of cohesive yielding at the maximum of the engineering stress $\sigma_{engr(max)}$.

Following the same protocol as used in a previous study[66] that elucidated the meaning of the stress overshoot in startup 'shear, we perform a set of elastic recovery experiments involving startup extension at different Hencky rates. Fig. 13a shows a series of startup extension and subsequent elastic recovery, covering a range of Wi_R from 0.25 to 2.5. Strikingly, there is nearly complete recovery before the engineering stress maximum $\sigma_{engr(max)}$ even for $Wi_R < 1$. For example, at $\dot{\varepsilon} = 0.01\ s^{-1}$, $\sigma_{engr(max)}$ occurs at $\varepsilon_{max} = 0.76$ (corresponding to an elongation ratio of $\lambda_{max} = 2.14$), *i.e.* it takes 76 s ($\ll \tau_d = 2578$ s at $T = 25\ ^\circ C$) to reach the maximum as shown in Fig. 13b. Since the Rouse time τ_R at 25 °C is only 25 s, 2/3 of this extension should be taking place under non-affine deformation conditions if chain retraction at τ_R actually took place. The 95% elastic recovery from a step extension of $\lambda = 2.14$ at $Wi_R = 0.25$ indicates that the extension of the entanglement network is well beyond a Hencky strain of 0.25, *i.e.*, beyond $\lambda = 1.28$. The lack of complete elastic recovery only occurs beyond λ_{max}. Thus, the data in Fig. 13a and b also reveal the significance of the engineering stress maximum as a signature of yielding of the entanglement network. Note that for $Wi_R = 2.5$, there emerges a local maximum first at $\lambda_{max} = 4.1$ as shown in Fig. 13a before the specimen eventually shows a monotonic increase until rupture. Even in this case, there is lack of full

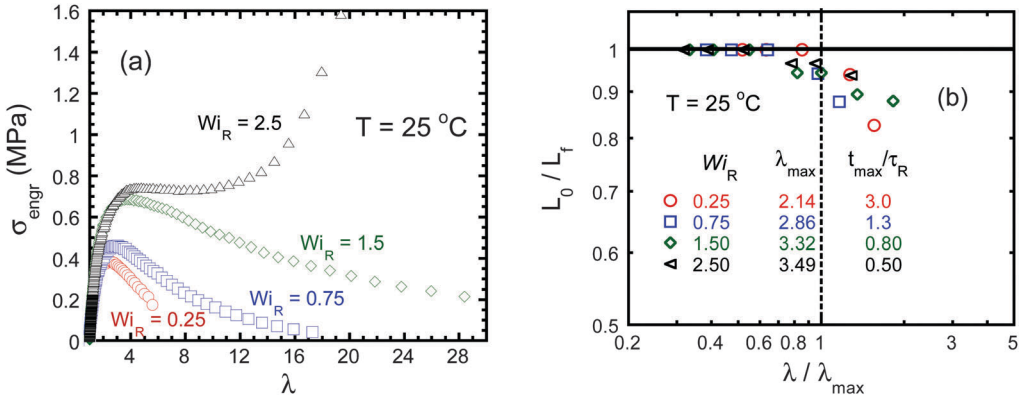

Fig. 13 (a) Engineering stress σ_{engr} *versus* stretching ratio λ for startup extension at four values of Wi_R at 25 °C. (b) The ratio of the initial specimen length L_0 to the final recovered length after it has been stretched to various elongation ratios both before and after the engineering stress maximum at λ_{max}, at four different Hencky rates of 0.01 to 0.1 at 25 °C where the Rouse time is 25 s.

elastic recovery beyond $\lambda_{max} = 4.1$ to indicate that the nature of the process after the first peak is viscoelastic. Future molecular dynamics (MD) simulation will clarify the molecular origin of the engineering stress non-monotonicity displayed in Fig. 13a.

Conclusions

We carried out three different types of homogeneous-deformation experiments to explore the existence of finite cohesion associated with chain entanglement. None of our experiments involves strain localization and non-quiescent relaxation and therefore can be more readily compared with the prevailing theoretical description. Specifically, step-wise shear and extension of moderate magnitude were performed to determine whether there is any sign of chain retraction to accelerate the stress relaxation. The observed lack of any speed-up in the stress relaxation independent of the deformation is consistent with the picture[64] that there is a cohesion barrier in the entanglement network. In other words, the nearly identical stress relaxation dynamics for step-wise shear with magnitude from $\gamma = 0.1$ to 0.7 and for step-wise extension from $\lambda = 1.2$ to 1.5 suggests that chain retraction did not occur. This assertion was made because the tube theory predicts an appreciably faster stress relaxation after any magnitude of step-wise deformation.

The state of chain entanglement after a step-wise extension is delineated during stress relaxation by a sudden application of a startup extension. The data analysis indicates that the geometric condensation associated with the affine extension still remains observable even after several reptation times τ_d let alone after merely one Rouse time τ_R, which is shorter than τ_d by a factor of 100. Finally, the full elastic recovery from step-wise extension, produced with $Wi_R < 1$ at any magnitude before the engineering stress maximum $\sigma_{engr(max)}$ is consistent with the idea that there is finite cohesion.

The results of the present study are consistent with the recent MD simulations[29–31] that have revealed significant chain stretching and lack of barrier-free chain retraction. Thus, the previous messages[33,78] remain valid that there is merit to explore a more realistic conceptual framework for the nonlinear rheology of entangled polymers.

Acknowledgements

The authors thank Dr R. Weiss for permission to use the TA ARES-G2 in his lab. The work is, in part, supported by NSF (DMR-1105135) and the National Natural Science Foundation of China (No. 21120102037, 21334007, and 21304097).

References

1 W. Graessley, *The entanglement concept in polymer rheology*, Springer, Berlin/Heidelberg, 1974.
2 J. D. Ferry, *Viscoelastic properties of polymers*, Wiley, New York, 1980.
3 P. G. De Gennes, *J. Chem. Phys.*, 1971, **55**, 572–579.
4 M. Doi and S. F. Edwards, *J. Chem. Soc., Faraday Trans. 2*, 1979, **75**, 38–54.
5 M. Doi and S. F. Edwards, *J. Chem. Soc., Faraday Trans. 2*, 1978, **74**, 1818–1832.
6 M. Doi and S. F. Edwards, *J. Chem. Soc., Faraday Trans. 2*, 1978, **74**, 1802–1817.
7 M. Doi and S. F. Edwards, *J. Chem. Soc., Faraday Trans. 2*, 1978, **74**, 1789–1801.
8 M. Doi and S. F. Edwards, *The theory of polymer dynamics*, Oxford University Press, New York, 1986.
9 H. Watanabe, *Prog. Polym. Sci.*, 1999, **24**, 1253–1403.
10 T. C. B. McLeish, *Adv. Phys.*, 2002, **51**, 1379–1527.
11 G. Ianniruberto and G. Marrucci, *J. Rheol.*, 2001, **45**, 1305–1318.
12 A. E. Likhtman and R. S. Graham, *J. Non-Newtonian Fluid Mech.*, 2003, **114**, 1–12.
13 A. E. Likhtman, S. T. Milner and T. C. B. McLeish, *Phys. Rev. Lett.*, 2000, **85**, 4550–4553.
14 G. Marrucci, *J. Non-Newtonian Fluid Mech.*, 1996, **62**, 279–289.
15 R. S. Graham, A. E. Likhtman, T. C. B. McLeish and S. T. Milner, *J. Rheol.*, 2003, **47**, 1171–1200.
16 M. W. Collis, A. K. Lele, M. R. Mackley, R. S. Graham, D. J. Groves, A. E. Likhtman, T. M. Nicholson, O. G. Harlen, T. C. B. McLeish, L. R. Hutchings, C. M. Fernyhough and R. N. Young, *J. Rheol.*, 2005, **49**, 501–522.

17 R. S. Graham, J. Bent, L. R. Hutchings, R. W. Richards, D. J. Groves, J. Embery, T. M. Nicholson, T. C. B. McLeish, A. E. Likhtman, O. G. Harlen, D. J. Read, T. Gough, R. Spares, P. D. Coates and I. Grillo, *Macromolecules*, 2006, **39**, 2700–2709.
18 D. J. Read, K. Jagannathan and A. E. Likhtman, *Macromolecules*, 2008, **41**, 6843–6853.
19 S. K. Sukumaran and A. E. Likhtman, *Macromolecules*, 2009, **42**, 4300–4309.
20 S. Q. Wang, *Macromol. Mater. Eng.*, 2007, **292**, 15–22.
21 S. Ravindranath and S. Q. Wang, *J. Rheol.*, 2008, **52**, 957–980.
22 P. E. Boukany, S. Q. Wang and X. Wang, *Macromolecules*, 2009, **42**, 6261–6269.
23 C. Chung, T. Uneyama, Y. Masubuchi and H. Watanabe, *Rheol. Acta*, 2011, **50**, 753–766.
24 P. D. Olmsted, *Rheol. Acta*, 2008, **47**, 283–300.
25 J. M. Adams and P. D. Olmsted, *Phys. Rev. Lett.*, 2009, **102**, 067801.
26 J. M. Adams, S. M. Fielding and P. D. Olmsted, *J. Rheol.*, 2011, **55**, 1007–1032.
27 M. Mohagheghi and B. Khomami, *ACS Macro Lett.*, 2015, **4**, 684–688.
28 Y. Lu, L. An, S.-Q. Wang and Z.-G. Wang, *Macromolecules*, 2015, **48**, 4164–4173.
29 Y. Lu, L. An, S.-Q. Wang and Z.-G. Wang, *Macromolecules*, 2014, **47**, 5432–5435.
30 Y. Lu, L. An, S.-Q. Wang and Z.-G. Wang, *ACS Macro Lett.*, 2014, **3**, 569–573.
31 Y. Lu, L. An, S. Q. Wang and Z. G. Wang, *ACS Macro Lett.*, 2013, **2**, 561–565.
32 S. Q. Wang, *J. Polym. Sci., Part B: Polym. Phys.*, 2008, **46**, 2660–2665.
33 S. Q. Wang, Y. Wang, S. Cheng, X. Li, X. Zhu and H. Sun, *Macromolecules*, 2013, **46**, 3147–3159.
34 K. Osaki, K. Nishizawa and M. Kurata, *Macromolecules*, 1982, **15**, 1068–1071.
35 K. Osaki, S. Kimura and M. Kurata, *J. Polym. Sci., Polym. Phys. Ed.*, 1981, **19**, 517–527.
36 K. Osaki, N. Bessho, T. Kojimoto and M. Kurata, *J. Rheol.*, 1979, **23**, 617–624.
37 K. Osaki and M. Kurata, *Macromolecules*, 1980, **13**, 671–676.
38 Y. Einaga, K. Osaki, M. Kurata, S.-i. Kimura and M. Tamura, *Polym. J.*, 1971, **2**, 550–552.
39 M. Fukuda, K. Osaki and M. Kurata, *J. Polym. Sci., Polym. Phys. Ed.*, 1975, **13**, 1563–1576.
40 Y. H. Wen and C. C. Hua, *J. Rheol.*, 2009, **53**, 781–798.
41 D. C. Venerus and R. Nair, *J. Rheol.*, 2006, **50**, 59–75.
42 K. Osaki, H. Watanabe and T. Inoue, *Macromolecules*, 1996, **29**, 3611–3614.
43 K. Osaki, E. Takatori, Y. Tsunashima and M. Kurata, *Macromolecules*, 1987, **20**, 525–529.
44 K. Osaki, S. Kimura, K. Nishizawa and M. Kurata, *Macromolecules*, 1981, **14**, 455–456.
45 F. A. Morrison and R. G. Larson, *J. Polym. Sci., Part B: Polym. Phys.*, 1992, **30**, 943–950.
46 R. G. Larson, S. A. Khan and V. R. Raju, *J. Rheol.*, 1988, **32**, 145–161.
47 M. T. Islam, J. Sanchez-Reyes and L. A. Archer, *J. Rheol.*, 2001, **45**, 61–82.
48 M. T. Islam and L. A. Archer, *J. Polym. Sci., Part B: Polym. Phys.*, 2001, **39**, 2275–2289.
49 T. Inoue, T. Uematsu, Y. Yamashita and K. Osaki, *Macromolecules*, 2002, **35**, 4718–4724.
50 T. Inoue and K. Osaki, *Nihon Reoroji Gakkaishi*, 2003, **31**, 207–212.
51 L. A. Archer, *J. Rheol.*, 1999, **43**, 1555–1571.
52 D. C. Venerus, *J. Rheol.*, 2005, **49**, 277–295.
53 K. Osaki, *Rheol. Acta*, 1993, **32**, 429–437.
54 L. A. Archer, Y. L. Chen and R. G. Larson, *J. Rheol.*, 1995, **39**, 519–525.
55 Y. Einaga, K. Osaki, S. Kimura, N. Yamada, M. Tamura and M. Kurata, *Polym. J.*, 1973, **5**, 91–96.
56 T. Kashyap and D. C. Venerus, *Macromolecules*, 2010, **43**, 5874–5880.
57 C. C. Hua, J. D. Schieber and N. C. Andrews, *Rheol. Acta*, 1997, **36**, 544–554.
58 C. C. Hua, J. D. Schieber and D. C. Venerus, *J. Chem. Phys.*, 1998, **109**, 10028–10032.
59 C. C. Hua and J. D. Schieber, *J. Chem. Phys.*, 1998, **109**, 10018–10027.
60 C. C. Hua, J. D. Schieber and D. C. Venerus, *J. Rheol.*, 1999, **43**, 701–717.
61 J. Neergaard and J. D. Schieber, *J. Non-Newtonian Fluid Mech.*, 2002, **105**, 111–130.
62 P. E. Boukany and S. Q. Wang, *Macromolecules*, 2009, **42**, 2222–2228.
63 G. Liu and S. Q. Wang, *Macromolecules*, 2012, **45**, 6741–6747.
64 S. Q. Wang, S. Ravindranath, Y. Wang and P. Boukany, *J. Chem. Phys.*, 2007, **127**, 064903.
65 S. Ravindranath, S. Q. Wang, M. Olechnowicz, V. Chavan and R. Quirk, *Rheol. Acta*, 2011, **50**, 97–105.
66 Y. Wang, X. Li, X. Zhu and S. Q. Wang, *Macromolecules*, 2012, **45**, 2514–2521.
67 R. S. Graham, E. P. Henry and P. D. Olmsted, *Macromolecules*, 2013, **46**, 9849–9854.
68 K. Osaki, T. Inoue and T. Isomura, *J. Polym. Sci., Part B: Polym. Phys.*, 2000, **38**, 1917–1925.
69 C. M. Vrentas and W. W. Graessley, *J. Non-Newtonian Fluid Mech.*, 1981, **9**, 339–355.
70 J. W. M. Noordermeer and J. D. Ferry, *J. Polym. Sci., Polym. Phys. Ed.*, 1976, **14**, 509–520.
71 L. R. G. Treloar, *The Physics of Rubber Elasticity*, Clarendon Press, Oxford, 3rd edn, 2005.
72 D. M. Sussman and K. S. Schweizer, *J. Chem. Phys.*, 2013, **139**, 234904.
73 H. Sun, P. Lin, G. Liu, K. Ntetsikas, K. Misichronis, N. Kang, J. Liu, A. Avgeropoulos, J. Mays and S.-Q. Wang, *J. Rheol.*, 2015, **59**, 751–767.
74 Y. Wang and S. Q. Wang, *J. Rheol.*, 2008, **52**, 1275–1290.
75 Y. Wang and S. Q. Wang, *J. Rheol.*, 2009, **53**, 1389–1401.
76 C. G. Robertson, S. Warren, D. J. Plazek and C. M. Roland, *Macromolecules*, 2004, **37**, 10018–10022.
77 X. Zhu and S. Q. Wang, *J. Rheol.*, 2013, **57**, 223–248.
78 S.-Q. Wang, *Soft Matter*, 2015, **11**, 1454–1458.